CHAPTER II
BACKGROUND AND LITERATURE SURVEY

2.1 Theoretical Background

For a vertical pipe, there are four main regimes, as shown in Figure 2.1 and 2.2, occurring successively at ever-increasing gas flow rates:

(a) *Bubble Flow*: There is a continuous liquid and the gas phase dispersed as bubble within the liquid continuum. The bubbles travel with complex motion causing the bubbles coalescing and generally are of non-uniform size.

(b) *Slug Flow*: This flow pattern, which, in vertical systems, is sometimes referred to as plug flow, occurs when the bubble size tends toward that of the channel diameter, and characteristic bullet-shaped bubbles are formed. A bubble surrounded by liquid thin film is often called a Taylor bubble. The liquid between the Taylor bubbles often contains a dispersion of smaller bubbles.

(c) *Churn Flow*: At higher gas velocities, the Taylor bubbles in slug flow break down into an unstable pattern in which there is a churning or oscillatory motion of liquid. This flow occurs more predominantly in wide-bore tubes and may not be so important in narrow-bore tubes where the region of churn flow is small.

(d) *Annular Flow*: This configuration is characterized by the liquid phase travelling as a film on the channel walls, and the gas phase flowing through the center. Part of the liquid can be carried as droplets in the central gas core.

(e) *Mist Flow*: The velocity of the continuous gas phase is so high that it reaches as far as the tube wall and entrains the liquid in the form of droplets.

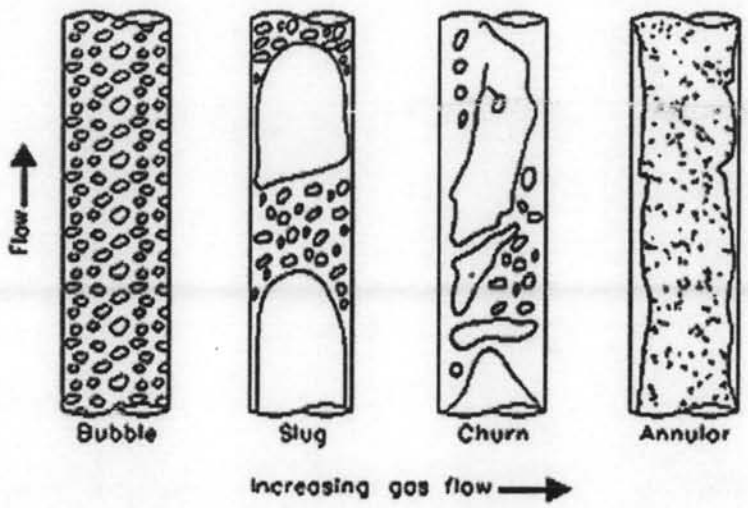

Figure 2.1 Modelling flow pattern transitions for steady Upward Gas-liquid Flow in Vertical Tubes (Bornea, and Dukler, 1980).

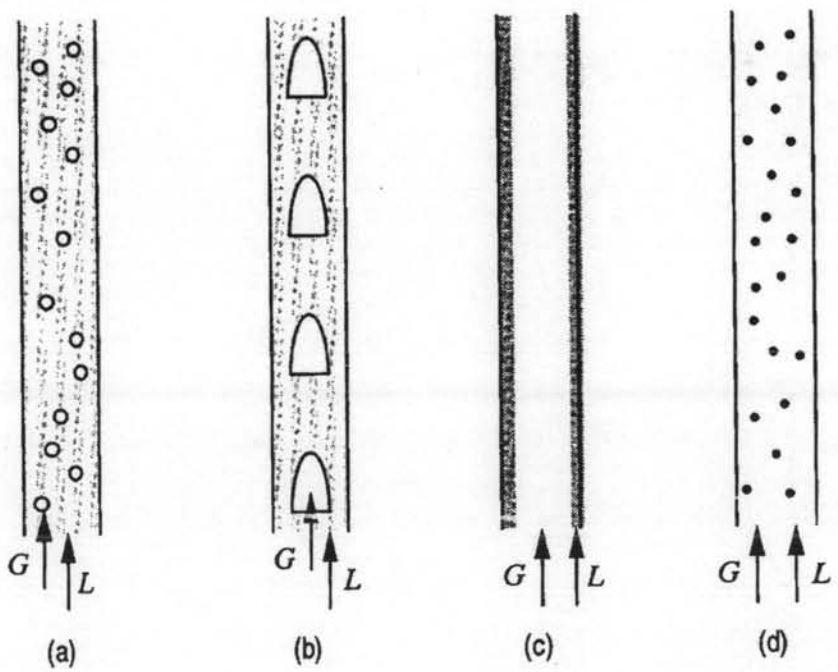

Figure 2.2 Two-phase flow regimes in a vertical tube: (a) bubble; (b) slug; (c) annular; and (d) mist flow. In each case, the gas is shown in white, and the liquid is shaded in black (Wilkes, 1999).

2.1.1 Determination of Flow Regime

A typical situation occurs when the gas and liquid volumetric flow rates G and L are specified, and the pressure gradient *dp/dz* and void fraction are calculated. Correlations for these last two variables are more likely to be successful if we can recognize the particular flow regime and develop relationships specifically for it. The following approximate demarcations are recognized:

2.1.1.1 Bubble/ Slug Flow Transition.

Small bubbles introduced at the base of a column of liquid will usually and eventually coalesce into slugs. The transition depends very much on the size of the bubbles, how they are introduced, the distance from the inlet, and on surface tension effects, so there is no simple criterion for the transition.

2.1.1.2 Slug/ Annular Flow Transition.

In the narrow gap between the gas and the tube wall at the base of the slugs, there is a significant downwards flow of liquids, and hence a fairly strong relative velocity between gas and liquid in the point. For increasing gas flow rates, the result is instability of the liquid film, which can start bridging the whole cross section of the tube. These bridges can in turn be broken up by the gas and the flow becomes chaotic.

2.1.1.3 Annular/ Mist Flow Transition.

The transition is ill-defined because most annular flow entrains some droplets.

2.1.2 Bubble Flow Regime

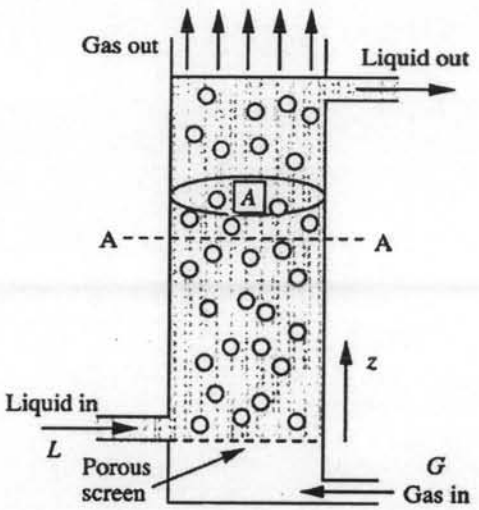

Figure 2.3 Bubble flow (Wilkes, 1999).

Gas bubbles and liquid in upward co-current flow are shown in Figure 2.3. The mean upward liquid velocity across plane A-A is

$$\bar{u}_l = \frac{G+L}{A} \tag{2.1}$$

where, G = Volumetric flow-rate of gas, ccm

L = Volumetric flow-rate of liquid, ccm

A = Cross-sectional area of a tube, cm^2

The rise velocity of gas bubbles below plane A-A are relative to a moving liquid which has a velocity ($\bar{u}_l$), so that velocity of the gas bubbles is:

$$v_g = \bar{u}_l + u_b = \frac{G+L}{A} + u_b \tag{2.2}$$

where u_b is the bubble velocity rising into a stagnant liquid. The bubble velocity, u_b rising into a stagnant liquid was proposed by Peebles and Garber (1953).

$$\text{Bubble velocity} = u_b = 1.00\sqrt{g\,R_b} \tag{2.3}$$

where g = gravitational acceleration constant (m/s^2), R_b = radius of sphere that has the same volume as the spherical-cap bubble (m) and total volumetric flow rate of gas is:

$$G = \varepsilon A v_g \tag{2.4}$$

So, the void fraction is given by:

$$\frac{G}{\varepsilon A} = \frac{G+L}{A} + u_b \qquad \text{or} \qquad \varepsilon = \frac{G}{G+L+u_b A} \tag{2.5}$$

The pressure gradient is given fairly accurately by considering only the hydrostatic effect. For the relatively low liquid velocities likely to be encountered in the bubble-flow regime, friction is negligible.

$$\frac{dp}{dz} = -\rho_l g(1-\varepsilon) \tag{2.6}$$

2.1.3 Slug Flow Regime

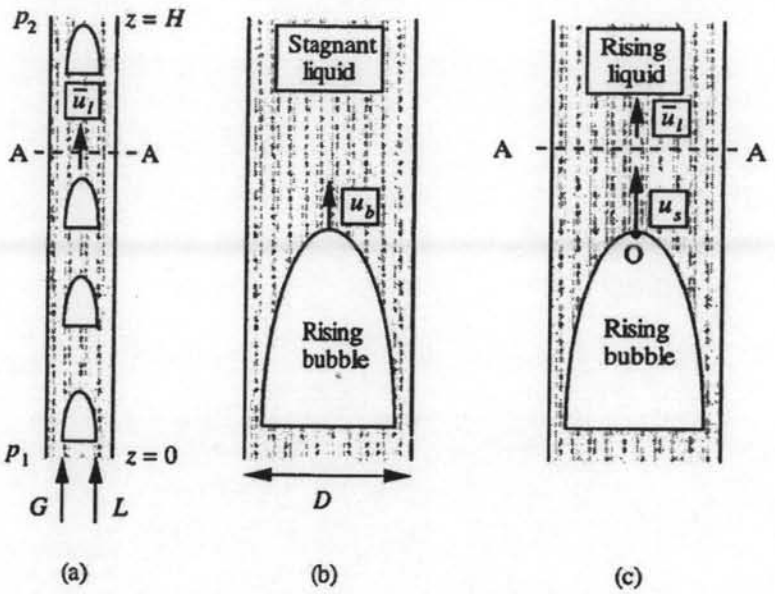

Figure 2.4 Two-phase slug flow in a vertical pipe: (a) ascending gas and liquid; (b) rising bubble in stagnant liquid; (c) rising bubble in moving liquid (Wilkes, 1999).

Figure 2.4(a) shows the gas and liquid flow upwards together at single volumetric flow rates G and L, in a pipe of internal diameter D. An upwards liquid velocity (u_l) across a plane A-A is leading of a gas slug. The total upward volumetric flow rate of liquid across A-A must be the combined gas and liquid flow rates which enter at the bottom. Therefore the mean liquid velocity at plane A-A is $\bar{u}_l = (G+L)/A$, in which A is the cross-sectional area of the pipe.

Figure 2.4(b) shows a different situation that of a single bubble is moving steadily upward with a rise velocity u_b in a stagnant liquid. Davies and Taylor (1950) used an approximate analytical solution for the non viscous liquid such as water and light oils, which is

$$u_b = c\sqrt{gD} \tag{27}$$

where the constant c = 0.33 and g is the gravitational acceleration. From the experimental data (The mechanics of large bubbles rising though extended liquids and though liquid in tubes), the constant c should equal to 0.35.

A slug rises in a stagnant liquid, as shown in Figure 2.4(b) and the highest velocity occurs at the center of the pipe-near the nose of the slug. Nicklin, Wilkes, and Davision (1962), showed that the value of liquid velocity of was about $1.2\bar{u}_l$, when the Reynolds numbers were greater than 8,000.

Hence, the true rise velocity of the slug is:

$$u_s = 1.2\frac{G+L}{A} + u_b = 1.2\frac{G+L}{A} + 0.35\sqrt{gD} \tag{2.8}$$

From the conservation of the gas; this gives:

$$G = u_s A\varepsilon \tag{2.9}$$

Substituting u_s in equation (2.9) to (2.8)

$$\frac{G}{\varepsilon A} = 1.2\frac{G+L}{A} + 0.35\sqrt{gD} \tag{2.10}$$

The equation (2.10) can be solved for the void fraction when the gas and liquid flow rates are known. It is very important to determine the pressure drop in a tube of height H. Also note that the weight of the liquid, which occupies a fraction (1-ε) of the total volume, is much greater than that of the gas. Therefore, the pressure drop is given to a first approximation by

$$p_1 - p_2 = \rho_L g H(1-\varepsilon) \tag{2.11}$$

A secondary correction to equation (2.11) would include the wall friction on the liquid "pistons" between successive gas slugs. Thus, if $(dp/dz)_{sp}$ is single-phase frictional pressure gradient for liquid only, flowing at a mean velocity $\bar{u}_l$, a more accurate expression for the pressure gradient is

$$\frac{dp}{dz} = (1-\varepsilon)\left[-\rho_l g + \left(\frac{dp}{dz}\right)_{sp}\right] \tag{2.12}$$

Sylvester (1987) showed the mechanistic model for calculating pressure gradient for slug flow. The mechanistic model for vertical slug flow is formulated based on the assumption that the flow is fully developed and stable. This assumption requires that the liquid slug and the Taylor bubble rise steadily without any relative velocity between them. The model is developed for a slug unit consisting of one Taylor bubble with its surrounding liquid and one liquid slug. The idealized slug unit is shown in Figure 2.5.

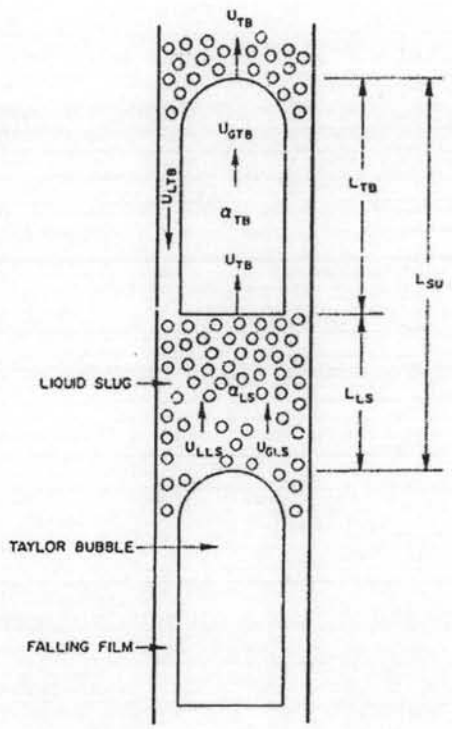

Figure 2.5 Slug unit (Sylvester, 1987).

Table 2.1 Model variables for Sylvester theory

L_{SU}	Length of the slug unit (m)
L_{TB}	Length of the Taylor bubble (m)
L_{LS}	Length of the liquid slug (m)
α_{TB}	Void fraction of the Taylor bubble
α_{LS}	Void fraction of the liquid slug
α_{SU}	Void fraction of the slug unit
U_{TB}	Velocity of the Taylor bubble (m/s)
U_{LTB}	Velocity of the liquid film around the Taylor bubble (m/s)
U_{GTB}	Velocity of the gas in Taylor bubble (m/s)
U_{GLS}	Velocity of the gas in liquid slug (m/s)
U_{LLS}	Velocity of the liquid in the liquid slug (m/s)

The large gas bubbles or Taylor bubbles occupy nearly the entire pipe cross section and translate steadily upward with a velocity, U_{TB}. For fully developed slug flows of low viscosity liquids, the ideal Taylor bubbles are long cylindrical voids having a spherical nose and a flat tail. Their length L_{TB} will remain constant in the axial direction provided expansion effects are negligible. The liquid film flows past the Taylor bubble with velocity, U_{LTB}. The Taylor bubble is followed by a liquid slug which contains numerous small gas bubbles. It is assumed that these small bubbles are distributed uniformly throughout the liquid slug with a void fraction given by α_{LS}. The length of the liquid slug, L_{LS}, also remains constant.

Stable slug flow is visualized to be continuous train slug units which move steadily upward along the pipe at a velocity U_{TB}. Although this is an idealized picture of vertical slug flow, it represents a fairly accurate model of the actual situation from a time-averaged point-of-view.

The total pressure drop in the slug unit consists of three components

$$(\Delta P)_T = (\Delta P)_A + (\Delta P)_H + (\Delta P)_F \qquad (2.13)$$

where

$(\Delta P)_T$ is total pressure drop in the slug unit (Pa)

$(\Delta P)_A$ is acceleration pressure drop (Pa)

$(\Delta P)_H$ is hydrostatic pressure drop (Pa)

$(\Delta P)_F$ is frictional pressure drop (Pa)

The acceleration pressure drop is taken to be that required to reverse the direction and accelerate the liquid film falling around the Taylor bubble to the velocity U_{LLS}. This pressure drop can be written as

$$(\Delta P)_A = \rho_L(U_{LTB} + U_{TB})(1-\alpha_{TB})(U_{LTB} + U_{TB} + U_{LLS}) \quad (2.14)$$

where

$$U_{LTB} = 9.916\left[gD\left(1-\sqrt{\alpha_{TB}}\right)\right]^{1/2} \quad (2.15)$$

$$U_{TB} = 1.2(U_{SG} + U_{SL}) + 0.35\left[\frac{gD(\rho_L - \rho_G)}{\rho_L}\right]^{1/2} \quad (2.16)$$

The hydrostatic pressure drop of the slug unit can be written in the form

$$(\Delta P)_H = \rho_L(1-\alpha_{LS})gL_{LS} \quad (2.17)$$

where

$$\alpha_{LS} = \frac{U_{SG}}{C_2 + C_3(U_{SG} + U_{SL})} \quad (2.18)$$

Thus equation (2.18) with $C_2 = 0.425$ and $C_3 = 2.65$ is chosen. It must be emphasized that although the form of equation (2.18) is theoretically sound, the coefficient were determined from a best least squares fit of Fernandes experiment data.

The frictional pressure drop of slug unit can be written as

$$(\Delta P)_F = \frac{L_{LS}}{2D}\left[\frac{\rho_G \beta f_{TB} U_{TB}^2}{(1-\beta)\left[1-(1-\alpha_{TB}^{1/2}\right]} + U_{LLS}^2 \rho_L (1-\alpha_{LS}) f_{LS} (1-\beta)\right] \quad (2.19)$$

where

$$\beta = L_{TB}/L_{SU} \tag{2.20}$$

f_{TB} is friction factor associated with the Taylor bubble. If it is assumed that the falling rough surface to the Taylor bubble, the Taylor bubble friction factor mat be written as

$$f_{TB} = \frac{1}{\left[-2.0\log\left\{\frac{\left(1-\alpha_{TB}^{1/2}\right)}{7.4}\right\}\right]^2} \tag{2.21}$$

f_{LS} is the friction factor associated with the liquid slug which in general depends upon the Reynolds number of the liquid slug , Re_{LS}, and the pipe roughness. This dependency can be expressed as

$$f_{LS} = f_{LS}\left(\mathrm{Re}_{LS}, \varepsilon/D\right) \tag{2.22}$$

where ε is the pipe roughness, and

$$\mathrm{Re}_{LS} = \frac{\rho_L\left(1-\alpha_{LS}\right)U_{LLS}D}{\mu_{LS}} \tag{2.23}$$

Since $\mu_L >> \mu_G$ equation (2.23) may be simplified to

$$\mu_{LS} \cong \mu_L\left(1-\alpha_{LS}\right) \tag{2.24}$$

Equation (2.22) can be expressed explicitly using the Zigrang-Sylvester equation which is an explicit which is an explicit representation of the Colebrook equation.

$$f_{LS} = \frac{1}{\left[-2.0\log\left\{\frac{\varepsilon/D}{3.7} - \left(\frac{5.02}{\mathrm{Re}_{LS}}\right)\log\left(\frac{\varepsilon/D}{3.7} + \frac{13}{\mathrm{Re}_{LS}}\right)\right\}\right]^2} \tag{2.25}$$

Substituting equation (2.14), (2.17) and (2.19) into equation (2.13) gives the total pressure drop for slug unit.

$$(\Delta P)_T = \rho_L (U_{LTB} + U_{TB})(1-\alpha_{TB})(U_{LTB} + U_{TB} + U_{LLS}) + \rho_L (1-\alpha_{LS}) g L_{LS}$$

$$+ \frac{L_{LS}}{2D}\left[\frac{\rho_G \beta f_{TB} U_{TB}^2}{(1-\beta)\left[1-(1-\alpha_{TB}^{1/2}\right]} + U_{LLS}^2 \rho_L (1-\alpha_{LS}) f_{LS} (1-\beta)\right] \qquad (2.26)$$

2.1.4 Churn or Froth Flow Regime

The froth flow pattern has been variously called churn, froth, wave entrainment, dispersed plug, and semi-annular. It is similar to the slug pattern in that the flow is pulsating and there are alternate slugs of gas and liquid. At the higher flow rates characteristic of froth flow, the bubble wakes become more agitated, a large number of small bubbles are torn off at the tail, and the whole wake becomes richer in bubbles. The froth pattern differs from the regular orderly slug flow pattern in that neither the bubbles of gas nor the slug of liquid maintain their identity as they moved up the tube.

The pattern occurs over a modest range of superficial gas velocities and apparently only up to a certain critical superficial liquid velocity. It is a transition pattern from the regular slug flow to the annular-mist flow. At any given liquid rate, the pattern extends from the point of breakdown of the regular liquid slugs and gas bubbles to a gas velocity sufficient to carry the bulk of the liquid up the wall of the tube by the surface drag exerted.

The froth flow pattern is not amenable to theoretical analysis and has not been the subject of any extensive experimental study.

2.1.5 Annular-Mist Flow Regime

The annular-mist flow pattern is widely encountered in the flow of gas-liquid mixtures at high gas rates and gas-liquid ratios. The annular-mist flow pattern in gas-liquid systems is characterized by an upward moving, continuous, and smooth to wavy film of liquid on the tube wall and a much more rapidly moving central core of gas, containing entrained droplets of liquid in a concentration which

may vary from low to high. The liquid film may be wholly in laminar motion or it may be laminar only nearest the wall, and turbulent nearest the gas-liquid interface.

Shearer and Nedderman (1965) divided the annular-mist flow pattern into the "small ripple" regime and the "disturbance wave" regime. In the small ripple regime, small waves develop on the liquid surface and move at velocities of the order of the interface velocities and then lose their identity. At higher liquid flow rates, the waves are larger, and they travel at velocities two to five times the interfacial velocity. These waves are known as disturbance waves.

At any given liquid rate, decreasing the gas rate causes more of the liquid to be present in the film, the liquid film velocity to decrease, and its thickness to increase. At a certain critical gas rate, the liquid film velocity becomes zero, and below this rate the liquid film has a negative velocity near the wall, and it penetrates the gas phase, and the froth flow occurs. As the gas rate is increased, turbulence takes place in the liquid film, the thickness of the film decreases, waves develop at the interface, and an increasing number of droplets are torn from the film and entrained in the gas. Eventually the continuous film is destroyed and almost all the liquid is transported as entrained droplets in the gas phase.

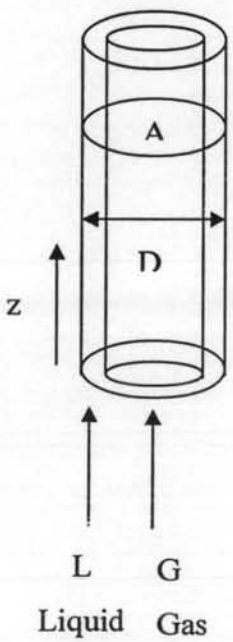

Figure 2.6 Vertical annular two-phase flow (Wilkes, 1999).

The simultaneous flow of gas and liquid in a vertical tube as shown in Figure 2.6. First, consider just the flow of gas in the inner core. Since the gas velocity v_g is typically much higher than that of the liquid, the pressure gradient may be approximated as if the gas were flowing with velocity v_g in a pipe of diameter D_g, giving:

$$\left(\frac{dp}{dz}\right)_{tp} = \left(\frac{dp}{dz}\right)_g = -\frac{2f_F\,\rho_g\,v_g^2}{D_g} - \rho_g g = \phi_g^2\left(\frac{dp}{dz}\right)_{go} - \rho_g g \quad (2.27)$$

Second, consider the entire flow, obtaining the frictional contribution from the viewpoint of the liquid:

$$\left(\frac{dp}{dz}\right)_{tp} = \phi_l^2\left(\frac{dp}{dz}\right)_{lo} - \left[\varepsilon\,\rho_g + (1-\varepsilon)\,\rho_l\right] g \quad (2.28)$$

For specified gas and liquid flow rates, the derivatives on the right-hand sides of both equations will be known by calculation. These equation can then be solved simultaneously for the two-phase flow pressure gradient $(dp/dz)_{tp}$ and the void friction ε.

2.2 Literature Survey

Mishima *et al.* (1996) studied characteristics of air-water two-phase flow in small diameter vertical tubes with inner diameters in the range from 1 to 4 mm. They found that void fraction was correlated well with the drift flux model with a new equation for the distribution parameter as a function of inner diameter. The rise velocity of the slug bubbles was also correlated well with the drift flux equation. The frictional pressure loss was reproduced well by Chisholm's equation with a new equation for Chisholm's parameter C as a function of inner diameter.

Chen *et al.* (1997) developed a new model for the transitions for slug flow to churn flow in vertical pipes. The transition is attributed to the wake effect of Taylor bubbles on highly aerated liquid slugs. The new model was compared with

existing models and published experimental data. It is in better agreement with experimental data than existing models, with respect to not only the basic trend of the transition boundary, but also its absolute location.

Costigan *et al.* (1997) identified slug flow regime from dynamic void fraction measurements in vertical air-water flow. An existing design of probe for the measurement of void fraction has been developed and tested. Distance of two meters was used to examine the dynamic variation of void fraction of air-water flows in a vertical 32 mm. diameter tube. Examination of the void fraction traces enabled the identification of six flow regime: discrete bubble flow occurs with local void fractions which depends upon the gas and liquid velocities but are at all time less than 0.45; spherical cap bubble flow consists of discrete bubble flow upon which irregular narrow void fraction peaks between 0.4 and 0.8 are superimposed; stable slug flow exists when liquid slug with void fraction of 0.8 or more; unstable slug flow occurs at relatively high liquid velocities which characterized by slug void fraction higher than 0.4 merging with Taylor bubble void fraction lower than 0.8; churn flow exists when many of the bubble/annular void fractions are below 0.8 but there are no low void fraction slugs remaining; annular flow exists if all void fractions are above 0.8.

Kawaji *et al.* (1997) investigated the flow structures of gas-liquid slug flow in a vertical tube. A photochromic dye activation method was used to obtain two-dimensional liquid velocity profiles around a Taylor Bubble rising in stagnant kerosene in a vertical 25.6 mm. I.D. pipe. A numerical simulation of the flow was conducted by using a Volume-of-Fluid (VOF) to predict both the shape of the Taylor bubble and the velocity profiles in the liquid phase. They also tested the hypothesis that a trailing bubble can accelerate, catch up and coalesce with a leading bubble because of lateral motion and reduced drag force, so, they did the experiment by using a solid Taylor bubble placed in a steady downward flow of liquid. They found that drag force decreases as the Taylor Bubble moves laterally, and this is considered to be important for explaining the acceleration and coalescence of Taylor Bubbles in vertical slug flow.

Luo *et al.* (1997) studied the interphase mass transfer in co-current vertical two-phase flow with non-Newtonian liquids by using aqueous solution of

Polyacrylamide (PAM) as the liquid phase, pure nitrogen as the gas phase, and oxygen as the transferred species. They found that at high liquid flow rates ($U_{LS} \geq$ 0.5 m/s) the volumetric mass transfer coefficient monotomically decreased with increasing polymer concentration. At low liquid flow rates ($U_{LS} \leq 0.1$ m/s) volumetric mass transfer coefficient decreased with increasing PAM concentration in the slug regime, and was insensitive to the polymer concentration in the churn regime.

Nigmatulin *et al.* (1997) studied the shape of Taylor bubble in vertical tubes. The experiment were carried out in the 1.5 m. vertical glass tube with 15.6 mm. inner diameter which was a part of loop where circulated distilled water. They compared the shape of the Taylor bubble with the theoretical knowledge they concluded that the theory gives a good agreement with their experiment except the waves, which are present on the surface of the Taylor bubble. The wave on the shape of the Taylor bubble is very important for calculating interfacial area density of the Taylor bubble. And this parameter is very important foe the mass, momentum and energy exchanges at the interface.

Cheng *et al.* (1998) investigated the structure of upwards air-water flow and its variation as the bubble-to-slug transition was approached in column of different diameters (28.9 and 150 mm. diameter), with a view to understanding the mechanism of the transition. From the experiment, they found that traditional slug flow did not exist in 150 mm. diameter column. Instead, there was a very gradual transition to a type of churn flow as gas rate was increased. Bubble size, both mean and median chord lengths, decreased with height and the bubble frequency increased. This suggests bubble break-up rather than coalescence, although there was some evidence of an increase in the maximum size of cap bubbles found at high gas rates. In the 28.9 mm diameter column, increasing the gas rate at constant liquid rate led to a sudden transition to slug flow with a jump in the gain factor to 1.0 and also in the SNR. The suddenness of the transition would suggest an instability mechanism, rather than a gradual coalescence. And the cause of the gradual transition in the 150 mm. diameter column remains unclear.

Talvy *et al.* (2000) carried out the experiments to determine the influence of the separation distance between two consecutive bubbles (liquid slug length) upon

the behaviour of the trailing bubble in vertical slug flow. They found that the trailing bubbles did not affect the motion of the leading one. The trailing bubbles acceleration was quiet prominent in the near wake of the leading elongated bubble. Even at distances exceeding 50 pipe diameters, vertical velocity field in the wake of the leading bubble affects the trailing bubble. These results are of particular importance for the estimation of the stable length and for modelling transient slug flow.

Farshad *et al.* (2001) developed new relative roughness charts along with corresponding mathematical equation for internally coated pipe. An integral part of the frictional pressure drop due to fluid flow in pipes involves the determination of absolute surface roughness and relative roughness. They found a new set of relative roughness charts for internally coated pipes and a relative roughness equation. These equations can be used in computer models and simulators for pressure drop calculation. The relative roughness charts and equation can be applied only to new and clean piping.

Furukawa and Fukano (2001) investigated the effect of liquid viscosity on the flow pattern of upward air-liquid two-phase flow. The experiments were carried out using water and aqueous glycerol solution as working fluid with up to 15 times change in liquid viscosity for isothermal, co-current, air-liquid, vertical upward flow in 19.2-mm. inner diameter tube. They found that liquid viscosity significantly affected the structure of the liquid film surrounding large bubble in slug flow and also those of waves formed on the liquid film in annular flow. From the flow pattern map, they found the transition line from bubble flow to slug flow significantly shifted to the smaller superficial gas velocity region with increasing liquid viscosity. But the transition line from the froth flow to the froth-annular flow and from the froth-annular flow to the annular flow moved to larger superficial gas velocity region with increasing liquid viscosity.

Song *et al.* (2001) studied the phase distributions for upward laminar bubbly flow with non-uniform bubble sizes. They found that a bubbly flow with non-uniform bubbles sizes have more complexes and varied phase distribution than uniform bubbles. The bubbles with different sizes had different phase distributions in the same bubbly flow. The different phase distributions for the small and large

bubbles created a more intense fluctuating flow field that suppressed the effect of the lateral force on the bubbles and then flattened void fraction profile peaks near the pipe wall.

Wongwises *et al.* (2001) determined the two-phase pressure drop, interfacial shear and shear stress and interfacial friction factor for two-phase air water upward concurrent flow in a 29 mm. inner diameter and 3 m. long vertical pipe. The interfacial friction factor was further determined by using the classical relationship between the interfacial shear stress and the interfacial friction factor. The changes in the air flow rate and the water film thickness have been found to have an effect on the interfacial friction factor. The interfacial friction factor has been approximated to be a function of superficial gas Reynolds number and the dimensionless film thickness.

Wolf *et al.* (2001) studied the flow development in vertical annular flow. The experiments were conducted in a 10.8 m. long tube of 31.8 mm. diameter. Local values of the pressure gradient, film thickness, wall shear stress, film flowrate, disturbance wave velocity and frequency were measured over a range of gas and liquid flowrates. The variation of these parameters with distance from the water inlet gives some idea of the flow development. From their experiment, it indicated that although the pressure gradient reached a steady value within the first 100 diameter or so for low air fluxes, it was still changing even after 300 diameters at high air and water flowrates. The higher pressure gradient at high flowrate may lead to a significant change in the air density and this may be the reason why the pressure gradient did not attain a steady value. The results from their experiments showed that annular flow takes considerable distance to develop. While all the important flow parameters showed appreciable variation in the region close to the inlet, they reached a quasi-steady state at different distances from the inlet.

Barbosa *et al.* (2002) studied the liquid entrainment, droplet concentration and pressure gradient at the onset of annular flow in a vertical pipe. The adiabatic air-water experiments were carried out in a vertical test section (31.8 mm. internal diameter, 10.8 m. long) in which an isokinetic probe was employed to measure the local mass fluxes of gas and of entrained liquid droplet in the core region; pressure gradient was also measured. Their studied the liquid entrainment in the region of the

transition between the churn and annular flow regimes in vertical gas-liquid flow. They found that, in the fully co-current annular region ($U_{GS}^{*} > 1$), the local droplet concentration was virtually constant within the gas core but in the region of transition between churn flow and annular flow the droplet concentration varied across the core. Both pressure gradient and entrained fraction exhibited a minimum at $U_{GS}^{*} \approx 1$, before increasing again in the annular regime.

Prasser *et al.* (2002) studied the evolution of the bubble size distribution in a vertical two-phase flow by using wire-mesh sensor. They found that the coalescence intensity depended on the local gas fraction. In case of the injection of bubbles small enough to be driven towards the wall, the formation of large bubbles started in the layer close to the pipe wall, where the gas fraction distribution developed the well-known wall peak. In case of a high enough gas fraction in the center, there can be a source of small bubbles in the central region, which afterwards started to move in direction toward the wall. So, theoretical models must therefore consider the different radial profiles of the gas fraction represented by different bubble size classes.

Xiaodong Sun *et al.* (2002) studied the interfacial area of bubbly flow in a relatively large diameter pipe. The measured parameters were local time-averaged void fraction, interfacial area concentration, bubble Sauter mean diameter, and interfacial velocity. The measurements were performed in a 101.6 mm. inner diameter pipe by four-sensor conductivity probe. These data were further used to evaluate the one-dimensional, steady state, one group interfacial area transport equation (IATE), which can serve as one of the constitutive relations for the two-fluid model. The agreement between the predictions from transport equation and the experiment measurement is reasonably good. The two groups IATE is recommended for general gas-liquid two-phase flow in various flow regimes.

Luo *et al.* (2003) investigated an expanded polystyrene particle and oil two-phase flows in a vertical pipe by using the three-dimensional PIT method. The experimental results show that the particles had almost the same distribution as spherical bubble in real bubbly flow. The major difference in phase distribution between real bubbly flows and the particle liquid flow may result from the

deformation of bubbles. Bubble deformation generated a smaller lift force and possibly a larger wall repulsion force which made the bubble volume fraction profile peak shift toward the pipe center and even produced a pipe center-peaked bubble volume fraction profile.

Malayeri *et al.* (2003) studied the results of void fraction for different temperatures by using neural network architecture based on three dimensionless groups as modified volumetric flow ratio, density difference ratio, and Webber number. The resultant network accurately predicts the void fraction with an over all average relative error of 3.6% for the training data and 5.8% for the unseen data. The trend of predicted void fraction is also consistent with those of the experiment. Their work demonstrates that neural networks in general may be a promising tool to the interpretation and analysis of two-phase flow data.

Dziubinski *et al.* (2004) investigated the flow pattern map of a two-phase non-Newtonian liquid-gas flow in the vertical pipe. The multi-phase mixture 5% water solution of carboxymethylcellulose (CMC) and suspensions of 2-17.8 wt% spherical glass particles in CMC solution were used as a continuous phase. To assess viscosity of a non-Newtonian liquid in two-phase flow and to compare its range with the viscosity of a Newtonian liquid, they used the effective viscosity to calculate. The results showed that flow rates of liquid and gas phase have a decisive effect on the flow structure being formed. They found that liquid viscosity started to affect greatly the type of flow structure only when the solution viscosity exceeding 100 mPa.s. The same flow structures were observed as in the case of two-phase Newtonian liquid-gas flow.

Satitchaicharoen and Wongwises (2004) investigated the flow patterns in vertical upward concurrent gas-liquid two-phase flow in mini-gap rectangular channels. The effect of gap size, channel width, and liquid viscosity on the flow patterns and flow patterns maps. The experiment carried by using air-water, air-20 wt.% glycerol solution, and air-40 wt.% glycerol solution flow in 5 different sized rectangular. The results showed that when channel width was fixed and the gap size was varied at a superficial liquid velocity, it is clear that the transition of each boundary also shifts to higher value of superficial air velocity. The same results were observed when gap size was fixed and channel width was varied. As liquid

with a higher viscosity was used , the CB-S transition line shifted to lower value of superficial air velocity while the S-C transition line and the C-A transition line shifted to a higher value of superficial air velocity. The flow pattern maps were based on the superficial velocities of air, water and glycerol solution all the transitions between two flow patterns were dependent on the fluid nature. Therefore, these maps may be not applicable to other fluids.

Wang *et al.* (2005) studied the two-phase slug flow across small diameter tubes with the presence of vertical U-type return bends. The translational velocity of the air slug across return bend usually peaked at an angle of ¶/2 to 3¶/4. They found that for slug flow entering at the lower tube with a total mass flux of 50 kg/m^2s and D is 6.9 mm having a small curvature ratio of 3, a flow reversal phenomenon was observed at the entrance region of the return bend. The flow reversal phenomenon was not seen if the flow entering at the top of the tube, instead, a very special "freezing slug" phenomenon is observed. But for D is 3 mm. the flow reversal and freezing slug phenomena were not seen.

Kliakhandler (2005) carried the experiment by use the hand soap and a small aquarium pump and bubbled air through the fluid. He discovered that air rising in liquid hand did not always produce discrete bubbles, instead, under certain conditions the air bubbles form long, stable, connected chain. In Newtonian liquids such connected sausage-link did not appear. The presence of long-chain polymers was critical to bubble-chain formation because the elastic properties of the polymers help the bubbles to stay connected.

Shen *et al.* (2005) tried to characterize the phase distribution patterns of two-phase flow in a vertical large diameter pipe. The phase distribution was linked with local parameters that governed the local flow condition, such as phase velocities, size distribution and configuration of bubble or interfaces. They measured for the interfacial parameters (void fraction, Sauter mean diameter and pressure loss) in a vertical upward air-water two-phase flow in a pipe with 0.2 m. in inner diameter and 24 m. in height by using the optical probe and different pressure transducers. They found that the phase distribution pattern in the vertical large diameter pipe can be divided into two basic patterns; namely, the wall peak and the core peak. With the application of the concept of skewness, the two-phase distribution patterns have been

quantitatively distinguished by establishing a phase distribution pattern transition criterion.

Okawa *et al.* (2005) studied the deposition rate and the entrainment rate of droplets for vertical upward annular two-phase flow in a small diameter tube. The test section was a round tube of 5 mm. inner diameter, air and water were used as test fluids and varied pressure between 0.14-0.76 mPa. They found that the deposition rate was primarily influenced by the droplet concentration in the gas core and the entrainment rate was correlated well with the dimensionless number denoting the ratio of interfacial shear force to surface tension force acting on the surface of liquid film. Their results were consistent with available empirical correlations that were developed using the experimental data for large diameter tubes.